Optical waveguides with apodized sidewall gratings via spatial-phase-locked electron-beam lithography

J. T. Hastings,[a] Michael H. Lim,[b] J. G. Goodberlet, and Henry I. Smith
Department of Electrical Engineering and Computer Science, Room 39-427, Massachusetts Institute of Technology, Cambridge, Massachusetts 02139

(Received 28 May 2002; accepted 23 September 2002)

We describe a technique to fabricate Bragg gratings in the sides of optical waveguides using a single lithographic step. This technique is particularly suited to the apodized gratings required for add/drop filters in dense-wavelength-division multiplexing. Apodization minimizes cross talk between channels and improves the filter response. Silicon-on-insulator rib waveguides with both uniform and apodized gratings were fabricated using direct-write spatial-phase-locked electron-beam lithography (SPLEBL). This approach combines SPLEBL's pattern-placement accuracy with the flexibility of direct-write device prototyping. The resulting grating-based devices exhibited substantially reduced side-lobe levels. © *2002 American Vacuum Society.*
[DOI: 10.1116/1.1521744]

I. INTRODUCTION

Optical data transmission is the only technology available to meet the demand for high-bandwidth, long-distance communications. As these communications networks grow in complexity, they will increasingly rely on compact, integrated components that manipulate signals in the optical domain. Not surprisingly, a number of integrated-optical components require diffraction gratings, periodic modulations of refractive index or physical structure, within an optical waveguide. Examples include distributed-feedback and distributed-Bragg-reflector lasers, gain equalization filters, dispersion compensators, and channel add/drop filters for wavelength-division-multiplexing (WDM) .

Often, uniform gratings do not provide the functionality or performance required for integrated-optical components. For grating filters designed to reflect a single channel within the WDM spectrum, reflections outside of the grating stop band must be reduced far below those of a uniform grating. The reduction of side lobes in the filter reflection spectrum is often termed apodization. In practice, one apodizes the reflection spectrum by gradually increasing and then decreasing the grating strength along the waveguide. For nonphotosensitive materials the grating is formed by varying the waveguide dimensions, and the grating's depth and duty cycle determine its strength. The fabrication process for apodized gratings must allow one or both of these parameters to vary.

Typically, a waveguide and grating are formed using separate lithographic steps, and the grating is placed in the top or bottom of the waveguide. In this case apodization can be introduced by varying the grating's duty cycle.[1] The weakest grating sections are defined by very narrow grating teeth; thus, the resolution of the lithographic method limits the minimum obtainable grating strength. Alternatively, if one places the grating in the sidewalls of the waveguide, both the waveguide and grating can be defined in a single lithographic step. Wong *et al.* have also produced uniform sidewall gratings in a two-lithographic step process.[2] Ideal apodization can be achieved with sidewall gratings by varying the extent to which the grating teeth extend into and out from the waveguide. The duty cycle can also be varied if necessary.

Proper device performance also requires that the grating remain spatially coherent over its entire length. Both stochastic and systematic spatial-phase errors contribute to out-of-band reflections, center-frequency shift, stop band broadening, and decreased peak reflectivity. Uniform gratings possessing the required long-range coherence are often produced by interference lithography, but this technique makes varying the grating strength difficult. Scanning electron-beam lithography's (SEBL) arbitrary-pattern exposure can directly introduce sidewall apodization, but standard SEBL tools exhibit inadequate pattern-placement accuracy for many grating-based devices. In spatial-phase-locked e-beam lithography (SPLEBL) the electron beam position is referenced to a spatially coherent fiducial grid on the substrate, generated by interference lithography.[3] Thus, SPLEBL combines the long-range spatial coherence of interference lithography with the arbitrary patterning capabilities of electron-beam lithography.

II. SILICON-ON-INSULATOR WAVEGUIDES

Placing gratings in the sidewalls of a waveguide is a general technique applicable to numerous devices and optical materials. Here we demonstrate sidewall gratings in silicon-on-insulator (SOI), a relatively unexplored materials system for Bragg-grating devices. Silicon exhibits low absorption at the communication wavelengths near 1550 nm. Optical confinement is provided by the silicon-dioxide layer below and air above. As a result, SOI provides an attractive materials system for integrated-optical components.

The high refractive-index contrast between silicon ($n_{Si}=3.48$ at 1550 nm) and silicon dioxide ($n_{SiO_2}=1.46$) dictates a maximum single-mode slab-waveguide thickness of

[a]Electronic mail: hastings@nano.mit.edu
[b]Currently with Clarendon Photonics, Newton, MA.

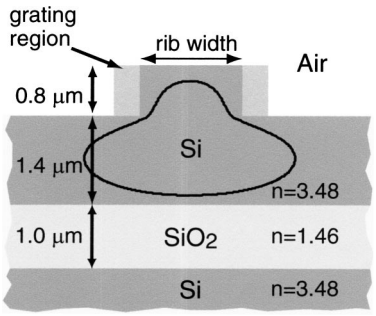

FIG. 1. Cross section of silicon-on-insulator rib waveguide with relevant dimensions and refractive indices. Depending on the desired local grating strength, the designed rib width varied from 1.60 to 1.48 μm and the grating width extended up to 520 nm on both sides. A contour of the modal power at -10 dB is overlaid on the diagram.

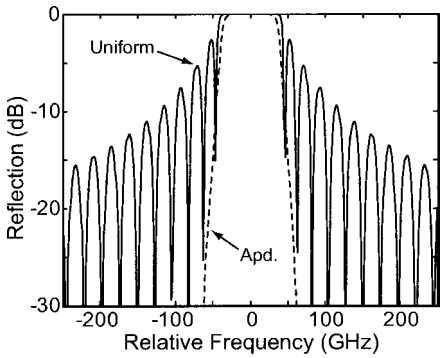

FIG. 2. Calculated reflection spectra for a 1.5-mm-long, uniform SOI grating (solid line) and a 3.0-mm-long SOI grating (dashed line) with raised cosine apodization; $\kappa_0 = 28\ \mathrm{cm}^{-1}$ for both gratings.

about 200 nm. Channel waveguides must be similarly constrained in at least one dimension. Such structures offer unmatched miniaturization, but they can exhibit high fiber coupling and propagation loss. Alternatively, rib waveguides can remain single moded with much larger mode sizes. Both Rickman, Reed, and Namavar and Schmidtchen *et al.* have fabricated single-mode SOI waveguides with dimensions of several microns and losses as low at 0.5 dB/cm.[4,5]

Placing gratings in a SOI waveguide introduces an additional constraint to the trade-offs among miniaturization, coupling efficiency, and propagation loss. For a large cross-section waveguide that is designed to couple well to optical fiber (mode diameters of ≈ 9 μm) a grating depth of hundreds of nanometers is too weak to obtain useful reflection responses. Smaller waveguide cross sections increase the mode's overlap with the grating and produce stronger coupling between the forward and backward traveling modes. As previously reported, waveguides with dimensions of 2–4 μm strike an effective compromise between coupling efficiency and grating strength.[6]

Figure 1 diagrams the cross section of the fabricated SOI waveguides. The silicon slab is 1.4 μm thick and the rib extends 800 nm vertically. The nominal rib width is 1.6 μm. A waveguide of these dimensions remains single moded and exhibits adequate grating strength. The SOI material was provided by Canon, Inc., using its commercial epitaxial layer transfer process (ELTRAN). This process combines epitaxial silicon growth, wafer bonding, and selective etching to produce thick silicon and silicon-dioxide layers with abrupt interfaces.

III. APODIZED SIDEWALL GRATING FILTERS

A waveguide mode is characterized by a propagation constant $\beta = 2\pi\bar{n}/\lambda_0$, where λ_0 is the free-space wavelength and $\bar{n}$ is the mode's effective refractive index. A perturbation of the waveguide's index or physical dimensions with spatial period $\Lambda = \lambda_0/2\bar{n}$ will couple forward and backward propagating modes for a narrow range of wavelengths about λ_0. Coupled-mode theory[7] relates the coupling strength, κ in cm^{-1}, between the forward and the backward propagating modes to the modal power integrated over the grating region and the refractive index profile of the grating. For a uniform grating of length L the peak reflectivity is given by

$$R_{\max} = \tanh^2(\kappa L). \tag{1}$$

When $\kappa L > 1$ the reflection bandwidth, in terms of frequency f, is

$$\Delta f \approx \frac{\kappa v_g}{\pi}, \tag{2}$$

where v_g is the group velocity of the mode.

While uniform gratings provide high reflectivity at the design wavelength they also exhibit large side lobes in the reflection spectrum. These reflections outside the stop band can introduce cross talk between nearby WDM channels. In general, one tailors the filter response of a grating by varying κ, $\bar{n}$, and/or Λ along the length of the waveguide.[8] We apodize the reflection spectrum by keeping $\bar{n}$ and Λ constant while gradually increasing and then decreasing κ.

To demonstrate the sidewall grating approach we designed a SOI waveguide-grating filter operating at 1550 nm with a reflection full-width of 60 GHz at -0.5 dB and 120 GHz at -30 dB, with no side lobes exceeding -30 dB. For $\bar{n} = 3.446$, the grating period is 224.9 nm For apodization, we chose the raised cosine function

$$\kappa(z) = \kappa_0 \cos^2\left(\frac{\pi z}{L}\right), \tag{3}$$

where the grating extends from $z = -L/2$ to $z = L/2$, $\kappa_0 = 28\ \mathrm{cm}^{-1}$, and $L = 3$ mm. Figure 2 compares the targeted apodized filter response to that of an unapodized grating with $L = 1.5$ mm and constant $\kappa(z) = \kappa_0$. Thus, the two gratings have the same integrated value of $\kappa(z)dz$.

We used a semivectorial finite-difference eigenmode solver to determine the dependence of κ and $\bar{n}$ on the waveguide and grating dimensions, for both TE and TM polarizations. For gratings in a high-index-contrast rib waveguide both κ and $\bar{n}$ are nonlinear functions of grating depth. As a result, the depth of the grating follows a different functional form than $\kappa(z)$. Figure 3(a) plots the inner and outer edges

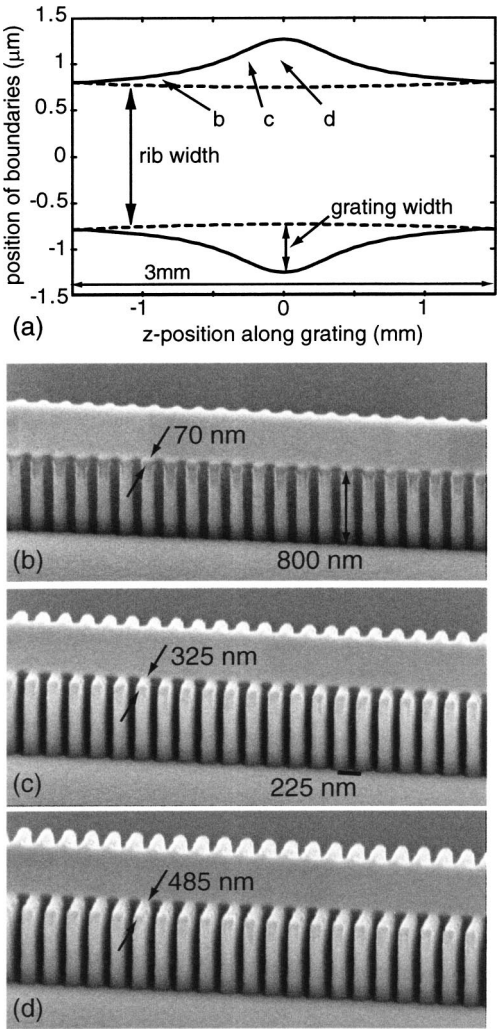

FIG. 3. (a) Boundaries of the waveguide rib and grating vs position along the length of the grating. This particular geometry provides a raised cosine apodization function. The rib narrows slightly as the grating depth increases in order to maintain a constant $\bar{n}$. (b),(c), and (d) are SEM images of an etched waveguide/grating structure at three locations along the grating, as indicated in (a).

of the grating region required to obtain $\kappa_0 = 28\ \mathrm{cm}^{-1}$ with constant $\bar{n} = 3.446$ for the TE mode. Rib waveguides exhibit inherent modal birefringence, and single-crystal silicon offers little compensating material birefringence. As a result, these devices are polarization sensitive, and would be used in a system that accounts for this.

Finally, the ends of the waveguides were curved to intersect the sample facet at an angle of 6.7°. This reduces multiple reflections between the chip facets and the grating, while allowing the facets to be polished normal to the SOI surface. This technique also requires the coupling angle between the optical fiber and the waveguide to be 24° to account for refraction.

IV. DEVICE FABRICATION VIA SPLEBL

Apodization greatly reduces the side lobes in the grating's reflection spectrum, but imperfections in the spatial phase of the grating also introduce undesirable reflections outside the stop band. It has been found, primarily in fiber-Bragg gratings, that periodic spatial-phase errors lead to additional discrete reflection peaks.[9,10] In addition, random spatial-phase errors increase out-of-band reflection over a broader range of wavelengths.[11]

Spatial-phase-locked electron-beam lithography (SPLEBL) offers a solution to the general problem of SEBL pattern placement and the specific problem of spatial-phase errors in integrated-optical gratings. SPLEBL positions the electron beam with respect to a fiducial grid located on the substrate. The beam positioning error is determined by measuring the spatial phase of the periodic grid. This error is fed back to the beam deflection system to create a closed control loop. As a result, stage-positioning errors, beam and/or stage drift, inaccurate field calibration, and numerous other placement error sources are compensated. The required fine-period, coherent, fiducial grid is produced by interference lithography. For the sidewall grating devices the critical dimension for placement accuracy lies along the device grating's k vector. Therefore, we need only perform spatial-phase locking in one dimension using a fiducial grating.

While several approaches to spatial-phase-locked e-beam lithography have been demonstrated,[12–14] the segmented-grid mode has proven particularly useful for optical devices.[15,16] In this mode the fiducial grid is isolated to unused areas of each deflection field. Before exposing each field the electron beam scans the grid and corrects for field shift, rotation, and scaling. This approach has been recently implemented on MIT's Raith 150 electron beam lithography system and was used to fabricate the devices described here.

An x-ray lithography mask with isolated 244 nm period fiducial gratings was previously fabricated by interference lithography specifically for integrated-optical devices.[15] This pattern was proximity printed in 200 nm of poly(methylmethacrylate) (PMMA) on a SOI substrate using a Cu_L-line electron-bombardment x-ray source. After developing the PMMA, 30 nm of tungsten was evaporated and lifted off by dissolving the PMMA in n-methyl pyrrolidone at 80 °C. The SOI substrate and tungsten fiducial grating were coated with 125 nm of hydrogen silsesquioxane (HSQ, commercially available as FOx from Dow Corning, Inc.) to be used as a negative e-beam resist.[17] The HSQ was pre-baked on hot plates for 120 s at 150 °C and again for 120 s at 220 °C.

The HSQ was exposed with a 30 kV electron beam and a dose of 620 $\mu C/\mathrm{cm}^2$ using segmented-grid SPLEBL. Figure 4 shows the secondary-electron signal obtained from the tungsten fiducial grating under the HSQ. The fine period and high signal-to-noise ratio allow precise phase locking. The pattern was exposed using a 89.9 μm field size (400 device grating periods), but no patterns were placed in the rightmost 18 μm of the field to avoid previously measured intrafield distortion.[18] We also observed a deflection-dependent field-scaling error after phase locking to the fiducial grating. The x scaling of the field was found to vary linearly with the beam deflection velocity in the y direction. This error was highly reproducible, and was compensated by a velocity de-

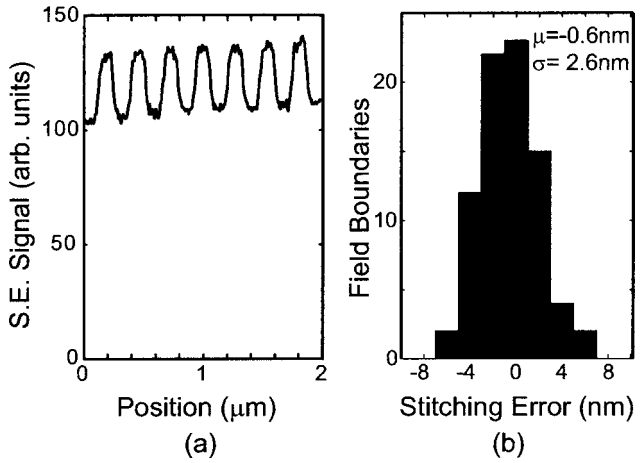

FIG. 4. (a) Secondary electron signal from the 30-nm-thick tungsten fiducial grating under 125 nm of HSQ resist (30 kV beam energy). (b) Histogram of the field-stitching errors from four SPLEBL-exposed SOI gratings. The mean error, μ, is -0.6 nm and the standard deviation, σ, is 2.6 nm.

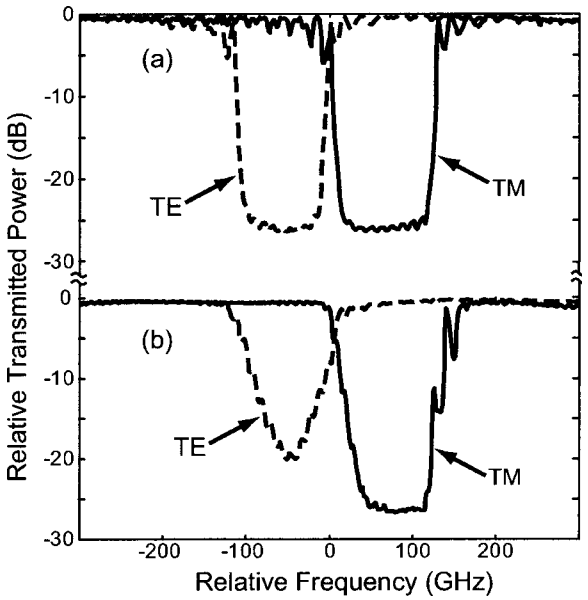

FIG. 5. Measured transmission response of a 1.5-mm-long, uniform SOI grating and a 3.0-mm-long SOI grating with raised cosine apodization. Both TE (dashed line) and TM (solid line) polarization states are shown. The center frequency corresponds to $\lambda = 1553.1$ nm. The TE and TM transmission minima are separated by ≈ 120 GHz.

pendent scale correction. After exposure, the HSQ was developed in a Shipley CD-26 developer for 8 min at 21 °C.

The pattern was transferred into the underlying silicon layer using chlorine reactive-ion etching (RIE) in a Perkin/Elmer sputtering system modified for RIE. The etch was carried out in four 3 min steps at a pressure of 10 mTorr, a dc self-bias of 350 V, and a power of 50 W. After etching, the grating teeth have an aspect ratio of 7:1 with little sidewall slope. The etch selectivity of Si to e-beam exposed HSQ was found to be $\approx 9{:}1$. The remaining HSQ etch mask was removed using hydrofluoric acid. Before testing, the devices were separated using a die saw and the end faces were polished.

V. DEVICE CHARACTERIZATION

We measured the stitching accuracy of segmented-grid SPLEBL by direct scanning electron microscopy (SEM) inspection of sidewall gratings patterned in HSQ. We used a discrete Fourier-transform algorithm to calculate the spatial phase (ϕ_1 and ϕ_2) of the grating on either side of the field boundaries. The stitching error is given by $\Lambda\ (\phi_2 - \phi_1)/2\pi$. For all sidewall-grating samples the standard deviation of the stitching error was found to be below 3 nm. After the deflection-dependent scaling error was compensated, the mean stitching error was -0.6 nm and the standard deviation was 2.6 nm [see Fig. 4(b)]. SPLEBL places each deflection field with respect to the fiducial grid, and the overall pattern placement error (σ_{pp}) can be deduced from the stitching measurement (σ_{st}). Thus, $\sigma_{pp} = \sigma_{st}/\sqrt{2}$, and the mean$+3\sigma$ pattern placement with respect to the fiducial grating is 6 nm. Because all vector-scan EBL systems have some deflection dependent pattern-placement error, this value may vary with pattern and exposure strategy.

The device's optical performance was characterized with a simple transmission measurement. Light from a tunable laser was coupled into the waveguide with a lensed optical fiber. Light from the waveguide output was collected with a microscope objective and focused through an aperture onto a photodiode detector. An intervening linear polarizer allowed us to measure the TE and TM polarization states independently. Transmission spectra were acquired by scanning the laser's output wavelength through the range of interest. The noise floor of the measurement was about 25 dB below the maximum transmitted power.

Figure 5 shows the transmission response for both 1.5-mm-long uniform gratings and 3.0-mm-long apodized gratings designed to have identical integrated values of $\kappa(z)dz$. The unapodized devices show the expected large side-lobe levels extending up to 5 dB below the maximum transmitted power. The bandwidths of the transmission minima (at -20 dB) are 96 and 113 GHz for the TE and TM modes, respectively.

The transmission spectra in Fig. 5(b) demonstrate the effectiveness of apodization in reducing side-lobe levels. While the out-of-band transmission is clearly reduced, the apodized devices show some anomalous behavior. The TE mode transmission minimum does not reach the noise floor, and the TM mode exhibits two points of increased transmission within the primary stop band. Both of these effects can be caused by symmetric chirp about the grating's midpoint. In this case, either the grating period or the effective index decreases as one proceeds toward the ends of the device from the center. Calibrated SEM measurements indicate that the grating width and the rib width deviate from the design by as much as 7% at the grating center. This deviation implies a symmetric chirp whose sign and order of magnitude are consistent with the measured transmission spectra.

VI. CONCLUSIONS

Placing Bragg gratings in the sidewalls of integrated waveguides allows the fabrication of grating-based devices in a single lithography step. This technique is applicable to a variety of devices and materials systems. In addition, sidewall gratings provide a particularly effective way to introduce apodization without varying the grating etch depth or duty cycle. We fabricated apodized sidewall gratings in silicon-on-insulator rib waveguides with grating strengths and apodization profiles suitable for WDM channel add/drop filters. Direct-write spatial-phase-locked e-beam lithography allowed the complex grating geometry to be patterned while maintaining a spatial coherence characteristic of interference lithography. The stitching errors present in the gratings were reduced to $\sigma = 2.6$ nm. The resulting device's transmission spectra showed greatly reduced side-lobe levels. Additional measurement and analysis are needed to quantify the waveguide/grating effective index variation and the devices' performance as reflection filters.

ACKNOWLEDGMENTS

The authors would like to thank Dr. Thomas Murphy, Tymon Barwitz, James Carter, and James Daley for their input and assistance. The authors also appreciate Dr. Falco C. M. J. M. van Delft's suggestions for using HSQ as an e-beam resist. The development of spatial-phase-locked e-beam lithography is supported under the DARPA/MTO program and ARO Grant No. DAAD19-99-1-0280.

[1]D. Wiesmann, C. David, R. Germann, D. Erni, and G. L. Bona, IEEE Photonics Technol. Lett. **12**, 639 (2000).
[2]V. V. Wong, W.-Y. Choi, J. M. Carter, C. G. Fonstad, and H. I. Smith, J. Vac. Sci. Technol. B **11**, 2621 (1993).
[3]J. Ferrera, M. L. Schattenburg, and H. I. Smith, J. Vac. Sci. Technol. B **14**, 4009 (1996).
[4]A. G. Rickman, G. T. Reed, and F. Namavar, J. Lightwave Technol. **12**, 1771 (1994).
[5]J. Schmidtchen, A. Splett, B. Schuppert, K. Petermann, and G. Burbach, Electron. Lett. **27**, 1486 (1991).
[6]T. E. Murphy, J. T. Hastings, and H. I. Smith, J. Lightwave Technol. **19**, 1938 (2001).
[7]A. Yariv and M. Nakamura, IEEE J. Quantum Electron. **QE13**, 233 (1977).
[8]K. O. Hill, Appl. Opt. **13**, 1853 (1974).
[9]J. Albert, S. Theriault, F. Bilodeau, D. C. Johnson, K. O. Hill, P. Sixt, and M. J. Rooks, IEEE Photonics Technol. Lett. **8**, 1334 (1996).
[10]C. Rogers, D. Goodchild, R. Baulcomb, M. Butler, P. Hoyle, S. Kanellopoulos, S. Clements, and B. Pugh, J. Vac. Sci. Technol. B **17**, 3217 (1999).
[11]R. Feced and M. N. Zervas, J. Lightwave Technol. **18**, 90 (2000).
[12]J. Ferrera, V. Wong, S. Rishton, V. Boegli, E. H. Anderson, D. P. Kern, and H. I. Smith, J. Vac. Sci. Technol. B **11**, 2342 (1993).
[13]J. G. Goodberlet, J. Ferrera, and H. I. Smith, J. Vac. Sci. Technol. B **15**, 2293 (1997).
[14]J. T. Hastings, F. Zhang, M. A. Finlayson, J. G. Goodberlet, and H. I. Smith, J. Vac. Sci. Technol. B **18**, 3268 (2000).
[15]M. H. Lim, T. E. Murphy, J. Ferrera, J. N. Damask, and H. I. Smith, J. Vac. Sci. Technol. B **17**, 3208 (1999).
[16]V. V. Wong, J. Ferrera, J. N. Damask, T. E. Murphy, H. I. Smith, and H. A. Haus, J. Vac. Sci. Technol. B **13**, 2859 (1995).
[17]F. C. M. J. M. van Delft, J. P. Weterings, A. K. van Langen-Suurling, and H. Romijn, J. Vac. Sci. Technol. B **18**, 3419 (2000).
[18]J. G. Goodberlet, J. T. Hastings, and H. I. Smith, J. Vac. Sci. Technol. B **19**, 2499 (2001).